CrossMark

RESEARCH ARTICLE

The hydrothermal alteration of cooling lava domes

Jessica L. Ball[1,2] · Philip H. Stauffer[3] · Eliza S. Calder[4] · Greg A. Valentine[1]

Abstract Hydrothermal alteration is a recognized cause of volcanic instability and edifice collapse, including that of lava domes or dome complexes. Alteration by percolating fluids transforms primary minerals in dome lavas to weaker secondary products such as clay minerals; moreover, secondary mineral precipitation can affect the porosity and permeability of dome lithologies. The location and intensity of alteration in a dome depend heavily on fluid pathways and availability in conjunction with heat supply. Here we investigate postemplacement lava dome weakening by hydrothermal alteration using a finite element numerical model of water migration in simplified dome geometries. This is combined with the rock alteration index (RAI) to predict zones of alteration and secondary mineral precipitation. Our results show that alteration potential is highest at the interface between the hot core of a lava dome and its clastic talus carapace. The longest lived alteration potential fields occur in domes with persistent heat sources and permeabilities that allow sufficient infiltration of water for alteration processes, but not so much that domes cool quickly. This leads us to conclude that alteration-induced collapses are most likely to be shallow seated and originate in the talus or talus/core interface in domes which have a sustained supply of magmatic heat. Mineral precipitation at these zones of permeability contrast could create barriers to fluid flow, potentially causing gas pressurization which might promote deeper seated and larger volume collapses. This study contributes to our knowledge of how hydrothermal alteration can affect lava domes and provides constraints on potential sites for alteration-related collapses, which can be used to target hazard monitoring.

Keywords Hydrothermal alteration · Lava dome · Lava dome collapse · Numerical modeling

✉ Jessica L. Ball
jlball@usgs.gov

[1] Department of Geology, University at Buffalo, 411 Cooke Hall, Buffalo, NY 14260-1350, USA

[2] United States Geological Survey, 345 Middlefield Road, Mail Stop 910, Menlo Park, CA 94025, USA

[3] Los Alamos National Laboratory, P.O. Box 1663, Los Alamos, NM 87545, USA

[4] School of GeoSciences, University of Edinburgh, The King's Buildings, Edinburgh EH9 3JW, UK

Introduction

Hydrothermal alteration of volcanic edifices promotes weakening and instability, increases the propensity for collapse, and can lead to significant volcanic hazards (Voight et al. 2002; Reid et al. 2002; McGuire 2003; Carrasco-Núñez et al. 2006; John et al. 2008; del Potro and Hürlimann 2009). The extent of alteration and magnitude of any resultant collapses ranges from those that involve parts of individual lava domes to major volcanic sector collapses (Siebert 2002). Here we focus on modeling hydrothermal alteration at the scale of an individual lava dome. Our motivation is that we know that hydrothermal systems in and around lava domes are pervasive, hazardous, and poorly understood. Lava dome internal structure can also be simplified for modeling in a reasonably valid way, which is significantly more difficult for larger, heterogeneous edifices.

Direct evidence of important hydrothermal systems associated with lava domes include (i) Soufrière systems, which are

🖄 Springer

commonplace around the bases of domes (Boudon et al. 1998; Walker et al. 2006; Bedrosian et al. 2007; Aizawa et al. 2009) and (ii) mass flow deposits (including debris avalanches and debris flow deposits) sourced from old domes, or dome complexes which contain a high proportion of altered material and clay-rich matrix (Opfergelt et al. 2006; Devoli et al. 2009). In fact, much of what we know about alteration in domes comes from the study of these mass flow deposits, where the hydrothermally altered components are no longer in situ, and their original position in the edifice can only be inferred indirectly from stratigraphy and flow reconstructions. Lava domes sit as variably permeable caps often directly above the volcanic conduits from which they were extruded. Such conduits may be the source of thermal and/or volatile fluxes for extended periods of time after an eruption has ceased (Bedrosian et al. 2007; Salaün et al. 2011). This configuration may render lava domes more susceptible to postemplacement alteration than other more widely dispersed erupted units. Indeed, a conduit-capping dome can host a hydrothermal system that would not otherwise exist had an eruptive phase resulted in a more exposed upper conduit.

Lavas within domes can be altered to secondary mineral assemblages (e.g., smectite clays, kaolinite, and alunite), weakening the edifice, reducing slope stability, and ultimately resulting in slope failure (Boudon et al. 1998; Opfergelt et al. 2006). Clay-rich alteration materials are not only low strength but have the potential to absorb and channel groundwater, locally increasing fluid pore pressure and promoting the expansion and/or formation of low-strength zones and exacerbating the risk of slope failure (Voight and Elsworth 1997). Secondary mineral formation (including hydrous silica) may also contribute to internal pressurization of lava domes by reducing gas permeability, thus provoking collapse through explosive decompression (Voight and Elsworth 2000). Upon collapse, clay-hosted pore water can lubricate mass flows, resulting in the generation of more mobile and cohesive debris flows than would be generated by collapse of dry material (Boudon et al. 1998; Reid et al. 2002; Opfergelt et al. 2006; John et al. 2008).

Two classic examples of edifice collapse involving hydrothermally altered lava domes/dome complexes are the 1998 event at Casita in Nicaragua (Scott et al. 2005; Opfergelt et al. 2006; Devoli et al. 2009) and the 1997 debris avalanche at Soufrière Hills, Montserrat (Sparks et al. 2002; Voight et al. 2002). In both cases low-strength, low-permeability alteration products are thought to have hosted water, which reduced the effective stresses in, and shear strength of, the rocks and which ultimately led to catastrophic destabilization of the edifices. At Casita, a ca. 8-ka dacite lava dome complex, a 1.6 million m^3 collapse on 30 October 1998 was triggered by intense rainfall associated with Hurricane Mitch. The collapse generated a debris flow and lahar that resulted in more than 2500 fatalities (Sheridan et al. 1999; Kerle 2002). The collapsed material was rich in smectite clays formed by intense hydrothermal

alteration of the original dacites (Opfergelt et al. 2006). A recent reanalysis of the collapse source area and deposits suggests that all failure surfaces formed at or near an interface between units of overlying volcanic breccia and underlying units of altered, clay-rich pyroclastic deposits and lavas. Clay contents in the altered units were estimated to be 38–50 wt% of the whole mass and more than 90 % of the fine fraction, with water contents in the remaining undisturbed clay-rich material ranging from 56 to 81 % (Devoli et al. 2009). For the 26 December 1997 debris avalanche at Soufrière Hills Volcano, Montserrat, hydrothermal alteration of the dome-retaining crater wall, itself made up of an older dome and pyroclastic deposits (Galway's Mountain/Soufrière, ~113 ka; Harford et al. 2002), was implicated as a major contributor to the destabilization and subsequent collapse and depressurization of the active lava dome (Sparks et al. 2002; Voight et al. 2002). The resultant debris avalanche deposits contained portions of the new dome but also between 6 and 15 wt% kaolinite and smectite group clays, alteration products typical of unsealed acid-sulfate hydrothermal systems. Intact avalanche blocks showed repeating layers of these alteration suites and suggested that the collapse slip surface intersected a layered hydrothermal system. The authors suggested that collapse mechanisms could have included an increase in pore-fluid pressure in the older dome materials due to the presence of low-permeability clay layers (Voight et al. 2002).

While collapses from a given, actively extruding (fresh) lava dome are common during an eruptive phase, those that result from postemplacement dome weakening by hydrothermal alteration are relatively infrequent, yet may pose very significant hazards that are harder to anticipate. The work reported here aims to increase our understanding of the collapse potential of young but inactive domes. Only sparse information exists on the collapse frequency of inactive, altered lava domes, either young or old. But the increasing number of mapped debris avalanche deposits (many of which source from lava dome complexes) and the similar posteruptive processes at work in both lava domes and larger volcanic edifices suggest that it is important to understand alteration in these systems. Salaün et al. (2011) and Le Friant et al. (2006) have mapped debris avalanche deposits and potential source areas on the Grande Découverte-Soufrière volcano and lava dome in Guadeloupe, which indicate that the recurrence interval of such collapses may be as high as one per 1000 years over the last 8 kyears. These collapses have resulted in debris avalanche deposits rich in hydrothermally altered material, and Salaün et al. (2011) suggest that hydrothermal alteration in the domes and flows that erupted after each collapse was rapid and widespread.

Geophysical and geochemical investigations have been used to characterize the hydrothermal system of specific lava domes at given points in time (Bedrosian et al. 2007; Finn et al. 2007; Finn and Deszcz-Pan 2011; Brothelande et al.

2014). Such studies are logistically challenging and cannot provide information about temporal variations of a system unless they are repeated. At the Mount St. Helens lava dome (Bedrosian et al. 2007), electrical resistivity surveys revealed that meteoric water circulated in the young dome due to heat input from a near-surface magmatic source, but did not capture longer term changes occurring in the hydrothermal system as the dome subsequently cooled. Aeromagnetic and electromagnetic surveys of Cascade volcanoes (Finn et al. 2007; Finn and Deszcz-Pan 2011) and the La Soufriere Volcano (Brothelande et al. 2014) have indicated the presence of water and altered material in specific locations in the edifices at the times of the surveys, but provide limited information about flow pathways within the hydrothermal systems and how they might be expected to have evolved or evolve in the future.
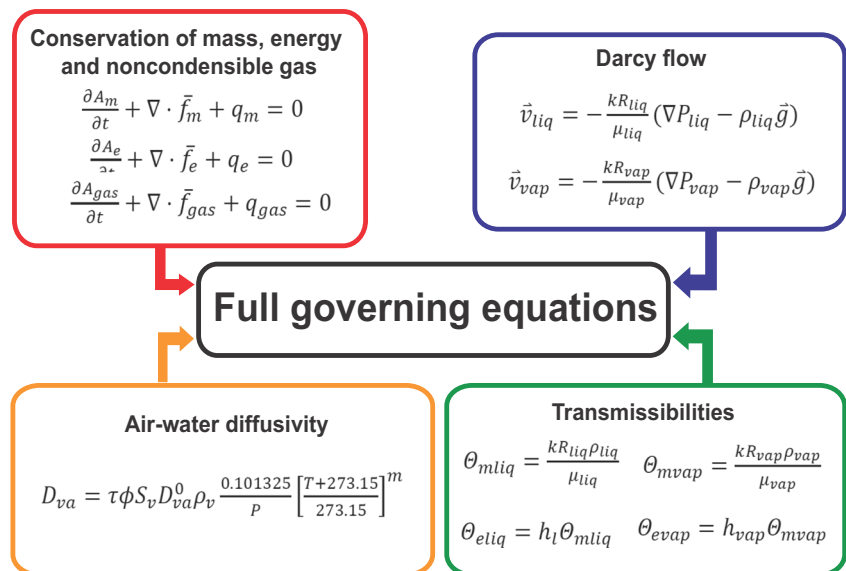
In this paper, we present a physics-based numerical model of heat and fluid flow in a generic lava dome combined with assessments of alteration potential, to determine where alteration is most likely to occur within a lava dome. The dynamics of hydrothermal flow and alteration processes in domes can be highly complex, and in detail, each dome is unique; we do not address all possible complexities but make a first step in quantitative modeling of major aspects of the systems. While we do not seek to address the specific type of alteration in this study, it is possible to distinguish likely regions of alteration based on knowledge of temperature gradients and fluid flux. We use this understanding to make some inferences about the different collapse styles and source areas that may occur in different hydrothermal settings. This work lays the groundwork for future investigations to identify likely alteration minerals, in order to distinguish whether individual collapses are related to weak alteration minerals (such as clays) or precipitation that reduce the porosity/permeability of the upper dome (such as silica).

Finite element heat and mass transfer code (FEHM)

The effect of meteorically derived water on the hydrothermal system of cooling lava domes is modeled using the finite element heat and mass transfer (FEHM) code. FEHM is an extensively validated (Zyvoloski et al. 1999; Dash et al. 2003; Dash 2003) porous flow simulator capable of modeling the flow of heat, water, air, and water vapor in a variably saturated porous and/or fractured medium at temperatures up to 1500 °C and fluid pressures of up to 1000 MPa. The code employs a Newton-Raphson scheme to iteratively solve discretized conservation equations for mass, energy, and momentum for fluid and vapor on a Voronoi-conforming finite-volume computational mesh (Miller et al. 2007; Zyvoloski 2007). Basic governing equations of state for conservation of mass and energy and modified Darcy flux are shown in Fig. 1; for a detailed derivation, see the Supplementary material. The temperature and pressure ranges of FEHM are ideal for modeling volcanic systems, and although it has previously been used to model cooling pyroclastic deposits (Keating 2005), volcanic seamount discharge and recharge (Hutnak et al. 2006), and mineral alteration in hydrothermal fault systems (Chaudhuri et al. 2009), it has never been applied to volcanic edifices or lava dome systems.

Active emplacement of a dome, whether endogenous or exogenous, is a principal forcing mechanism for collapse (Calder et al. 2002, 2005). However, in systems where emplacement has paused or ceased, other forcing mechanisms, including environmental ones, come into play (Calder et al. 2005; Barclay et al. 2006). Our focus here is on young but inactive/cooling lava dome systems. The rationale for this choice includes a number of considerations. First, only in inactive domes is hydrothermal alteration likely to play a significant role in collapses, and the relevant alteration minerals are most stable at temperatures of

Fig. 1 Basic equations that combine to form the full governing partial differential equations in FEHM, as reported in Zyvoloski et al. (1999). For a full derivation and comments, see the Supplementary material

Conservation of mass, energy and noncondensible gas

$$\frac{\partial A_m}{\partial t} + \nabla \cdot \bar{f}_m + q_m = 0$$

$$\frac{\partial A_e}{\partial t} + \nabla \cdot \bar{f}_e + q_e = 0$$

$$\frac{\partial A_{gas}}{\partial t} + \nabla \cdot \bar{f}_{gas} + q_{gas} = 0$$

Darcy flow

$$\vec{v}_{liq} = -\frac{kR_{liq}}{\mu_{liq}}(\nabla P_{liq} - \rho_{liq}\vec{g})$$

$$\vec{v}_{vap} = -\frac{kR_{vap}}{\mu_{vap}}(\nabla P_{vap} - \rho_{vap}\vec{g})$$

Full governing equations

Air-water diffusivity

$$D_{va} = \tau\phi S_v D_{va}^0 \rho_v \frac{0.101325}{P}\left[\frac{T+273.15}{273.15}\right]^m$$

Transmissibilities

$$\Theta_{mliq} = \frac{kR_{liq}\rho_{liq}}{\mu_{liq}} \qquad \Theta_{mvap} = \frac{kR_{vap}\rho_{vap}}{\mu_{vap}}$$

$$\Theta_{eliq} = h_l\Theta_{mliq} \qquad \Theta_{evap} = h_{vap}\Theta_{mvap}$$

200 °C or less (Ball et al. 2013; Giggenbach 1992). Second, in this initial application of FEHM, we required a relatively simple system where lava extrusion and its associated heterogeneous mass and thermal fluxes can be negated. Furthermore, restricting the simulations to lower temperatures (<200 °C) allows us to neglect high-temperature heat sources, which cause sudden short-term phase changes that increase model instability and prevent convergence on a solution for the governing equations (Ingebritsen et al. 2010).

Modeling methods

Our simulations are run for 100 years on a simplified lava dome geometry consisting of five material regions: a narrow conduit, a solid dome core, a clastic dome carapace or talus (covering and also tapering into a wedge away from the dome), a solid substrate, and a colluvium overlying the substrate (Fig. 2). The conduit radius was selected based on inferences made for actual domes as well as rheological models of dome eruptions (Fink and Pollard 1983; Costa et al. 2007). Previous models of dome growth and evolution (Fink and Griffiths 1998; Hale 2008; Hale et al. 2009a, b) and structural relationships of existing lava domes (Wadge et al. 2009) were used to design the configuration of the material regions used in our models. Two dome geometries are represented: a "crater-confined" dome similar to the domes at the Santiaguito lava dome complex in Guatemala (Ball et al. 2013), which provided some of the original motivation for this study, and a "perched" dome, essentially erupting on a sloping substrate whose core and talus are unconfined by a crater wall, similar to that of the Unzen or Merapi lava domes (Smithsonian Institution 1991; Anderson et al. 1999; Nakada et al. 1999; Walter et al. 2013). These dome geometries were investigated to determine if there was a difference in fluid migration when the dome was confined by a crater wall vs. unconfined.

Voronoi-conforming finite-volume computational meshes of these geometries were generated with the LaGriT Grid Generation Toolset, which was developed at Los Alamos National Laboratory (Fields et al. 1996; Miller et al. 2007).

LaGriT accepts input files consisting of coordinate data defining material regions, as well as commands choosing the level of discretization in those regions (or in other subregions specified by the user). The dome meshes for this study use a two-dimensional axisymmetric coordinate system; each mesh is a slice from the center of a dome, including a thick substrate that is extended down to several thousand meters in order to avoid boundary effects. The crater-confined and perched dome models are triangulated to (i.e., to have a spatial resolution of) 20 m within the top 1500 m of the dome and substrate; the remaining (lower) 1000 m of the mesh are triangulated to 40 m to save computational time and allow FEHM to calculate processes in the dome on a more detailed scale.

Material properties (density, porosity, initial permeability, specific heat, and thermal conductivity) of each dome region were taken from ranges given in the literature, summarized in Table 1. All values were chosen from lithologies commonly associated with lava domes (dome rocks, lava flows, and block and ash flow deposits) of andesitic and dacitic composition. In most of these studies, the values were determined from hand sample and drill core analyses. Where literature values had a wide range, a restricted range was chosen for modeling based on the most commonly found values. A complete record of the values from which these ranges were defined may be found in the Supplementary material.

Although the boundaries of large lava dome structures such as shear lobes are well described (Fink and Griffiths 1998; Watts et al. 2002), there is a limited amount of structural information available on the geometry of smaller, denser fracture networks in domes or their carapaces (i.e., the orientation, depth of penetration, concentration of fractures in a given area, aperture width of the fractures). Therefore, in this study, we have chosen to treat material regions as continua where the properties of the porous and/or fractured medium are averaged to account for variations that are not captured in our mesh. The appropriateness of a continuum approach depends on the ratio of the fracture density scale to the flow region scale. Khaleel (1989) modeled two-dimensional planar laminar flow through the columnar-fractured Columbia River Basalt Group lava flows and determined that for interconnected networks of filled/unfilled fractures of uniform aperture and column diameters of 1 m, continuum models were appropriate for length scales of at least 6 times the column diameter. That author also indicated that a continuum approach could be appropriate for other fractured rock masses if the entire rock mass is at least 6 times the smallest spacing of the fractures and preferably ~20–30 times the spacing in the case of variably sized and distributed fracture networks. The scale of fracturing and structural features on a lava dome is much smaller than the scale of dome and immediate substrate (even shear lobes of ten to a few hundred meters can be considered close to the 1/6th cutoff point), and so we feel that the continuum approach is reasonable for our simplified domes.
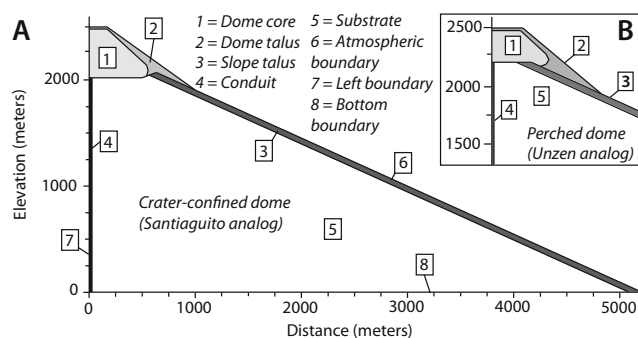

Fig. 2 Schematic of the two modeling grids for **a** crater-confined lava domes (e.g., Santiaguito) and **b** perched lava domes (not confined by a crater, e.g., Unzen)

Table 1　Summary of ranges for material properties derived from the literature review

Independent variable	Dome range	Talus range	Notes	References
Porosity (φ)	0.1–0.5	0.1–0.6	Talus layers are likely to be more porous than core (porosity increases with increasing fragmentation, void space)	García et al. (1989), Ingebritsen and Hayba (1994), Alt-Epping and Smith (2001), Barmin et al. (2002), Hurwitz et al. (2003), Keating (2005), Bartetzko et al. (2006), Flint et al. (2006), Scheu et al. (2006), Bernard et al. (2007), Mueller et al. (2008), Watanabe et al. (2008), Ikeda et al. (2008), Aizawa et al. (2009), Hicks et al. (2009), Wicks et al. (2011)
Permeability (m^2)	1.0×10^{-19} to 1.0×10^{-12}	1.0×10^{-17} to 1.0×10^{-10}	Talus layers are likely to be much more permeable (connected to porosity; see previous) due to higher porosity, fractured/rubbly state	Sammel et al. (1988), Sekioka (1988), Ingebritsen and Hayba (1994), Barmin et al. (2002), Keating (2005), Bartetzko et al. (2006), Bernard et al. (2007), Mueller et al. (2008), Watanabe et al. (2008), Aizawa et al. (2009), Hicks et al. (2009), Platz et al. (2012)
Density (kg/m^3)	593–2890	–	Dome and talus are assumed to be composed of the same material	García et al. (1989), Smith et al. (2001), Hurwitz et al. (2003), Keating (2005), Scheu et al. (2006), Bernard et al. (2007), Watanabe et al. (2008), Ikeda et al. (2008), Hicks et al. (2009)
Thermal conductivity (W/m K)	0.537–3.430	0.35	Value for most volcanic rocks is ~2	Sekioka (1988), García et al. (1989), Ingebritsen and Hayba (1994), Hurwitz et al. (2003), Keating (2005), Hicks et al. (2009)
Specific heat (J/kg K)	730–1557	2036	Dome and talus are assumed to be composed of the same material	Keating (2005), Hicks et al. (2009), Platz et al. (2012)

Precipitation/recharge

Because the actual elevation of water tables within volcanic edifices is not well constrained (Hurwitz et al. 2003), we initiate model runs for these domes by assigning complete saturation. Variable saturation is then allowed to develop as the simulation runs. This assumption is considered reasonable for volcanic systems/domes located in a tropical region that receive significant (i.e., >1000 mm/year) amounts of precipitation, such as the lava dome volcanoes detailed in Table 2. Previous models of groundwater in volcanoes using similar recharge and permeability values (Join et al. 2005; Hurwitz et al. 2003) show that water tables may rise to high levels within an edifice. As such, it is a reasonable assumption that there may be conditions under which a lower temperature (cooling) lava dome could become almost entirely saturated (for example, during an intense precipitation event). Even if there is an unsaturated zone in the immediate rubbly surface of the dome, the models would be unable to represent it if it was smaller than the 20-m mesh spacing. Given the paucity of information on water tables associated with lava domes, water saturation is taken as a reasonable first-order approach.

　Ground surface recharge in the models (1300 mm/year, or ~4.16×10^{-7} m³/[m² s]) is approximated using yearly precipitation rates in tropical regions. Actual infiltration rates into a dome would be expected to be less than precipitation due to evaporation, vegetation, localized impermeable surfaces, and runoff, but such variations would be site specific, localized, and impractical to represent in these simulations. Additionally, Rad et al. (2007) state that infiltration in volcanic settings with exposed fresh lavas and pyroclastic flows may be as high as 80 %. Thus, we consider that using a recharge value at the low end of measured precipitation rates for five existing domes in tropical to temperate climate regions is a reasonable proxy for infiltration (Table 3).

Boundary and initial conditions

For simplicity of the simulations, a number of material properties and boundary conditions were held constant throughout the simulations (Table 3). These include porosity, density, thermal conductivity, and specific heat of the material region, and pressure, temperature and recharge along the atmospheric surface (zone 6, Fig. 2). FEHM automatically treats the boundaries of the modeling mesh as impermeable unless otherwise specified, so left side (zone 7, Fig. 2) and basal (zone 8, Fig. 2) no-flow boundary conditions are assigned in these simulations. This reflects a radial dome geometry and a dome-topped volcanic edifice resting on an impermeable base (equivalent to plutonic or metamorphic rock, which can have permeabilities as low as 1×10^{-16} to 1×10^{-18} m²; Brace 1984).

　Initial conditions for the material regions in all simulations are detailed in Table 4. Initial rock permeabilities are divided

Table 2   Yearly precipitation rates for different currently active, or recently active, lava domes

Dome/location	Min rate (mm/year)	Max rate (mm/year)	Average (mm/year)	References
Soufrière Hills Montserrat, West Indies	1250	2000	1625	Barclay et al. (2006), Hemmings et al. (2015)
Soufrière of Guadeloupe, Guadeloupe, West Indies	??	10,000	10,000	Le Friant et al. (2006)
Merapi Central Java, Indonesia	2000	4500	3250	Lavigne et al. (2000)
Casita, Nicaragua			1250	Velázquez and Gómez-Sal (2007)
Unzen, Japan	2000	2600	2300	Ogawa et al. (2007)
Galeras, Columbia			1200	Meteorologia Aeronautica (Instituto de Hidrologia, Meteorologia y Estudios Ambientales) di Columbia (http://www.meteoaeronautica.gov.co/)
Santiaguito, Guatemala	1800	4000	2900	Lopez (2004)

into "low" permeability system (1.0×10^{-15} m^2 core and substrate, 1.0×10^{-13} m^2 talus), "intermediate" permeability system (1.0×10^{-14} m^2 core and substrate, 1.0×10^{-12} m^2 talus), and "high" permeability system (1.0×10^{-13} m^2 core and substrate, 1.0×10^{-11} m^2 talus) values. Two thermal conditions are used for simulations. One condition allows the dome and conduit to cool over time from their initial temperature conditions (specified in Table 4 for each material region). The other maintains a constant 200 °C heat source in the conduit, simulating a recharging magmatic heat source such as a dike or other intrusion providing heat to the system, slow solidification with release of latent heat, or heat fluxing from outgassing. Relative permeabilities vary with time and saturation according to a linear formulation (Zyvoloski et al. 1999; Zyvoloski 2007) which uses a residual liquid saturation of 0.2 and a residual vapor saturation of 0.1 (see Supplementary material for linear function equations). Again,

we focus here on low-temperature domes because adding fluids to the model under high-temperature conditions results in the model attempting to simulate abrupt phase changes and substantially slows the modeling process. High temperatures may also result in extremely low saturations in the modeling domain, which again slow calculations. We also note that the temperature of formation of many of the minerals of concern with respect to edifice weakening and instability (particularly smectite clay) falls within the 100–300 °C temperature range, which makes this a logical point in the temperature evolution of a cooling dome to investigate. At higher temperatures, the alteration mineral suite changes significantly and becomes dominated by minerals like biotite, actinolite, chlorite, and silica polymorphs (Henley and Ellis 1983; Reyes 1990), which are not usually implicated in alteration-related edifice collapse.

Alteration potential determined with the rock alteration index (RAI)

Volumetric liquid and vapor fluxes are calculated directly within FEHM, while temperature gradients are postprocessed based on the FEHM temperature fields. The temperature field and liquid volumetric flux vectors are then used to calculate alteration potential with the RAI for all nodes in the models at regular time intervals for each simulation. The RAI was developed to describe the likelihood of alteration processes occurring based on temperature gradients and patterns of fluid migration in subsurface aqueous reservoirs. Steep temperature gradients along flow paths promote alteration by inducing thermodynamic instability in the system and encouraging the formation of secondary minerals in equilibrium with thermal conditions (Raffensperger and Vlassopoulos 1999; Wetzel et al. 2001). The RAI is calculated from the temperature gradient and the fluid volumetric flux:

Table 3   Constant simulation parameters and boundary conditions

Parameter	Value
Porosity of zones 2 and 3	0.3
Porosity of zones 1 and 5	0.2
Porosity of zone 4	0.1
Initial temperature of zone 1	150 °C
Initial temperature of zone 2	30 °C
Initial temperature of zone 3	30 °C
Initial temperature of zone 4	200 °C
Initial temperature of zone 5	70 °C
Permeability of zone 4	1×10^{-16} m^2
Thermal conductivity of all units	2.0 W m^{-1} K^{-1}
Rock density of all units	2600 kg m^{-3}
Specific heat	1000
Atmospheric temperature (zone 6)	25 °C
Atmospheric pressure (zone 6)	0.1 MPa
Precipitation rate (zone 6)	1700 mm/year

$$\text{RAI} = \mathbf{q} \cdot \nabla T \qquad (1)$$

Table 4 Individual simulation parameters

Run	Geometry	Permeability dome talus (zone 2) (m^2)	Permeability dome core (zone 1) (m^2)	Permeability slope talus (zone 3) (m^2)	Permeability substrate (zone 5) (m^2)	Conduit heat
1	Crater-confined	1×10^{-12}	1×10^{-13}	1×10^{-12}	1×10^{-13}	Initial heat only
2		1×10^{-13}	1×10^{-14}	1×10^{-13}	1×10^{-14}	
3		1×10^{-14}	1×10^{-15}	1×10^{-14}	1×10^{-15}	
4	Crater-confined	1×10^{-12}	1×10^{-13}	1×10^{-12}	1×10^{-13}	200 °C sustained
5		1×10^{-13}	1×10^{-14}	1×10^{-13}	1×10^{-14}	
6		1×10^{-14}	1×10^{-15}	1×10^{-14}	1×10^{-15}	
7	Perched	1×10^{-12}	1×10^{-13}	1×10^{-12}	1×10^{-13}	Initial heat only
8		1×10^{-13}	1×10^{-14}	1×10^{-13}	1×10^{-14}	
9		1×10^{-14}	1×10^{-15}	1×10^{-14}	1×10^{-15}	
10	Perched	1×10^{-12}	1×10^{-13}	1×10^{-12}	1×10^{-13}	200 °C sustained
11		1×10^{-13}	1×10^{-14}	1×10^{-13}	1×10^{-14}	
12		1×10^{-14}	1×10^{-15}	1×10^{-14}	1×10^{-15}	

where **q** is the fluid volumetric flux (volume per cross-sectional area per time ($m^3/(m^2$ s)), and T is the temperature (°C). High positive values of the RAI coincide with areas of higher fluid flux and/or flow paths of rapidly increasing temperature and would promote mineral dissolution. High negative values are found in areas of higher fluid flux and/or flow paths of rapidly decreasing temperature and would promote mineral precipitation. A RAI value of zero does not necessarily reflect zero fluid flow, but can also indicate flow along isotherms. It should be noted that the RAI as calculated is an indicator of alteration potential only; it can be combined with geochemical species models to determine the likelihood of specific mineral formation, but for this initial study, we focus only on alteration potential.

Results

Twelve simulations were undertaken, varying the thermal and permeability conditions for each of the two dome geometries as described previously (Table 4). Temperature results highlight the differing evolution of temperature profiles in domes with a heat source and without, as in dome eruptions where magma either remains in some reservoir beneath the dome or has withdrawn. Variable permeability conditions were investigated because permeability is a primary control on fluid flux (both direction and intensity); we are also trying to represent differences in permeability between materials as well as cover the overall range of reasonable permeabilities based on rock property measurements (see previous section). As temperature distribution and fluid flux are the dependent variables by which the alteration indices are calculated, knowing how they vary in space and time allows us to comment on why certain patterns of RAIs develop.

Temperature gradients and liquid/vapor flux patterns

The highest temperatures in the simulations persist in areas that are initially warm (dome cores and conduits) and decrease over time; higher-than-background temperatures progressively migrate downward into the substrate (Fig. 3). In both dome geometries, domes with lower initial permeabilities tend to cool slower and do not achieve background temperatures by the end of the simulations, while initially higher permeability domes cool more rapidly, reaching background temperatures by or before the 100-year time limit. Likewise, in domes without a maintained heat source, both the onset of cooling as well as reaching background temperatures occurs earlier than for domes with a heat source. A persistent 200 °C heat source in the conduit generally allows the lower portions of the domes to remain hotter for longer periods of time, provided permeabilities are low. The inner cores of the domes remain hot longer in simulations with conduit heat, but there is little effect on outlying areas of the dome and talus. Crater-confined domes cool more slowly than perched domes, with perched domes cooling completely by the 50-year mark, whereas crater-confined domes still retain zones of elevated temperatures in their cores (Fig. 3e, f) One persistent feature in every simulation is the development of a zone of warmer temperatures (usually about 40–70 °C) at the base of the dome (Fig. 3c, d, initial development), which migrates toward the break in slope created by the intersection of the dome talus and slope talus. These zones develop faster in domes with medium or high permeabilities, but persist longer in lower permeability domes.

Liquid flux patterns are dominated by gravitational flow and show no evidence of convection (Fig. 4). The highest liquid fluxes (up to an order of magnitude higher than the recharge flux) are found in both the talus of both the dome and slopes throughout the 100-year simulations; liquid fluxes decrease where liquid saturations are low. In most simulations,

Fig. 3 a–h Temperature outputs
for the crater-confined (*left*) and
perched (*right*) dome geometries
after 1 year for intermediate
permeabilities and a conduit heat
source (figures illustrate a subset
of the full modeling domain
above 1500 m elevation)
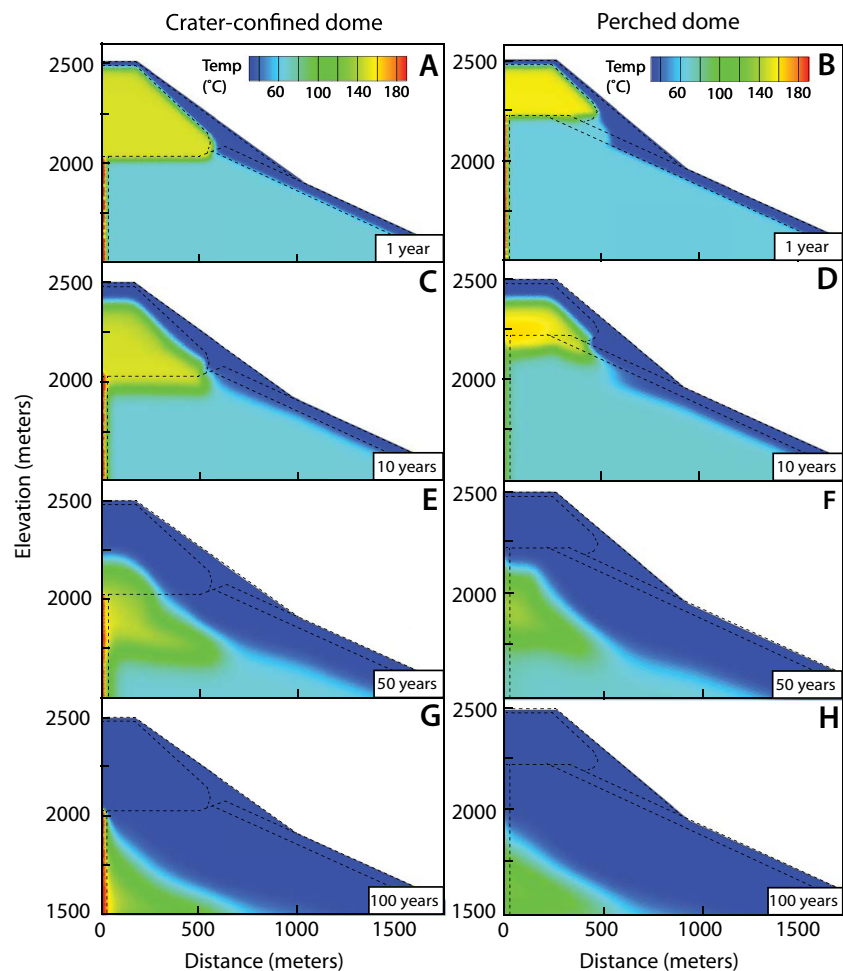
this decrease occurs at a front which migrates from the top of the dome core (Fig. 5a, b) to its center, and around the head of the conduit (Fig. 5g). Over time, high fluid fluxes decrease to background levels. Overall, fluxes vary between much less than the meteoric influx (min ~1.0×10^{-8} m³/m² s) to an order of magnitude higher. Maximum fluxes occur in simulations where the initial permeabilities are high (1.0×10^{-12} m² for talus, 1.0×10^{-13} m² for dome core and substrate). Perched domes contain larger areas of higher fluxes (Fig. 4b) than crater-confined domes (Fig. 4a), which coincide with the location of talus layers beneath the domes. These talus layers divert flow noticeably under the perched domes (Fig. 4d–h), while in crater-confined domes, this effect is much less pronounced and not as long lived (Fig. 4e). Adding a 200 °C heat source to the models does not appear to have a significant effect on fluid fluxes (i.e., through increasing buoyancy of fluids, etc.), but indirect factors like low saturation zones related to a heat source (which reduce relative permeability and thus fluid flux) may be masking lesser effects.

Vapor fluxes (Fig. 5) appear at the beginning of a simulation, and a boiling point front (Fig. 5a, b) migrates from the core/talus interface at the summit of the dome into the core of

the dome as time progresses (Fig. 5c–f). This front follows the high-temperature gradient between the hot core of the dome and the recharge-cooled carapace. Once the dome has cooled, vapor fluxes are confined to the area around the conduit head (Fig. 5e–g), although they only persist in simulations where the conduit is maintained at high temperature. The addition of a persistent heat source does not increase the strength of the vapor fluxes but does affect the fluxes indirectly (by increasing the areas that are not fully saturated and thus increasing the area over which vapor fluxes are produced). Vapor volume fluxes range from 1.0×10^{-6} to 9.0×10^{-6} m³/m² s and are higher when overall permeabilities are higher. Vapor fluxes are initially higher in crater-confined domes than perched domes (Fig. 5a, b), but more widespread in perched domes. By the 50-year mark, vapor fluxes in both domes are approximately the same magnitude (Fig. 5e, f).

Resulting alteration potential

Alteration potential (Fig. 6) in both domes is controlled primarily by the magnitude and direction of fluid flux and the temperature gradients of the cooling domes, and is thus

Fig. 4 a–h Fluid flux outputs for crater-confined and perched dome geometries at 1-, 10-, 50-, and 100-year intervals for intermediate permeabilities and a conduit heat source. *Blue* indicates higher fluxes and *green* lower fluxes. Streamlines indicate flow direction only and are arbitrarily spaced
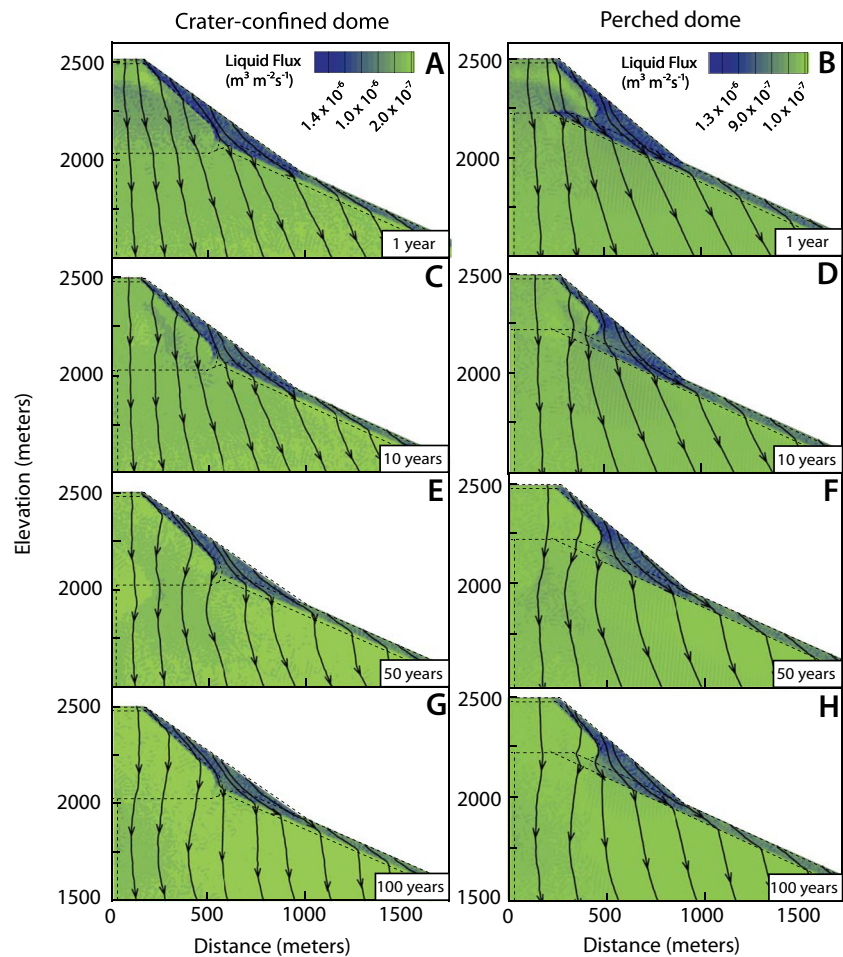
intimately related to permeability contrasts in materials and the availability of heat. Because the highest liquid fluxes occur in the higher permeability talus layers (Fig. 4a, b) and the greatest temperature gradients are generated between the dome cores and the cooler substrates (Fig. 3a, b), the highest positive and negative RAI values occur at the interface between the core and talus of the dome (Fig. 6a, b). High positive values at the dome summits suggest potential for mineral dissolution (alteration). Conversely, high negative values at the base of the dome and around the slope break in the talus indicate potential for mineral precipitation. Crater-confined domes show more intense positive and negative RAI values initially (Fig. 6a, b) and are the only geometry that still shows nonzero RAI values in the core of the dome by the 10-year simulation time (Fig. 6c, d). Neither geometry has nonzero RAI values in the dome after the 50-year simulation time (Fig. 6e–h).

Permeability and thermal conditions also control the strength and longevity of alteration zones. Potential alteration is more intense with low to moderately high permeabilities, but is not sustained for long unless a conduit heat source is present. Alteration potential decreases dramatically in these

models within even the first 10 years (Fig. 6c, d). However, very high permeabilities preclude strong alteration at the talus/ core interface, and instead, high RAI values are only generated around the conduit. Lower permeabilities combined with a heat source sustain both positive and negative RAI values longer, but at lower intensities than those developed at higher permeabilities. In both dome geometries, negative RAI values at the base of the dome tend to persist longer than the positive ones in the upper dome (Fig. 6c, d). The ideal combination for forming sustained, localized areas with high RAI values (positive or negative) appears to be a maintained conduit heat source combined with low to intermediate permeabilities (1×10^{-14} m^2 for core and substrate and 1×10^{-13} m^2 for talus). This enables water flux across strong temperature gradients without allowing the dome to cool too quickly.

Discussion

Domes cool from 150 to ~30 °C within 100 years in these simulations, suggesting that the lifetime of a low-temperature

Fig. 5 a–h Vapor flux outputs for crater-confined and perched dome geometries at 1-, 10-, 50-, and 100-year intervals for intermediate permeabilities and a conduit heat source. Higher fluxes are indicated by *red* and areas of zero vapor flux by *white*
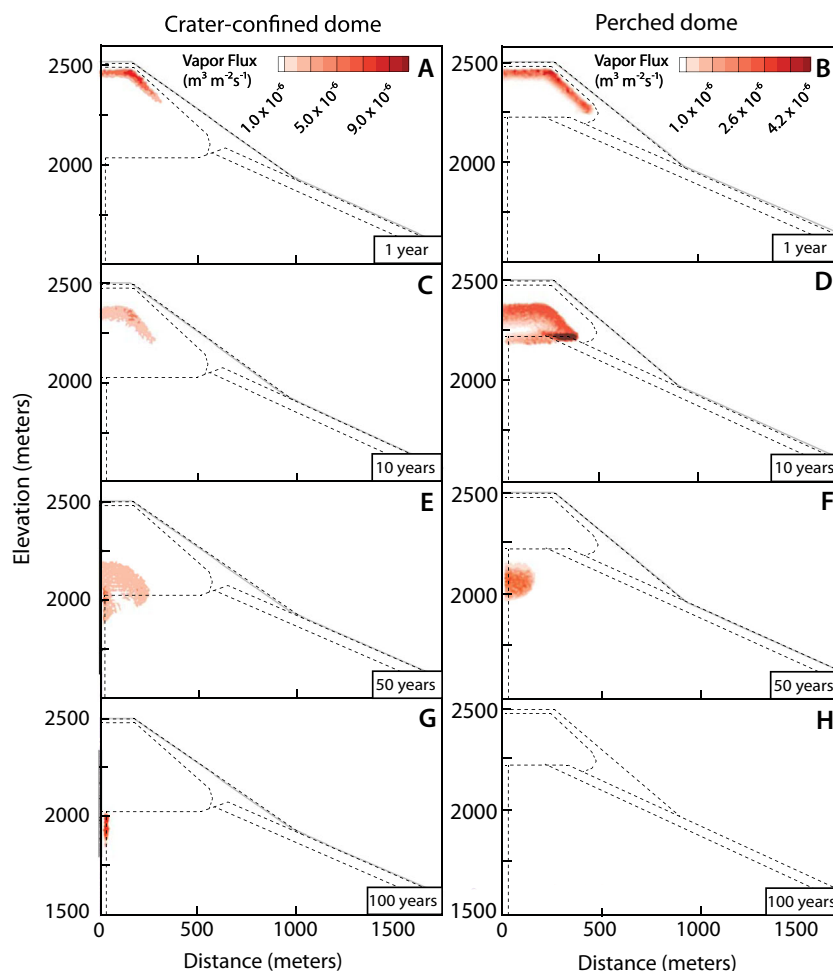

hydrothermal system in a tropical lava dome is only years to decades if the dome lacks a sustained high-temperature magmatic heat source. A sustained 200 °C heat source prolongs cooling, but 200 °C appears to be insufficiently hot to effectively drive hydrothermal circulation within the domes. Perched dome geometries cool faster than crater-confined domes, likely due to the presence of high-permeability talus layers beneath portions of the dome that allow more water transport around the dome core.

Overall, higher permeabilities and fluid fluxes promote more intense early-onset RAIs; however, these values are not as persistent as those in domes of lower permeabilities. Crater-confined geometries retain intense RAIs somewhat longer than perched domes because of the presence of high-permeability talus layers beneath perched domes (which helps cool the domes faster), but geometry exerts a much weaker control than permeability. Therefore, early-onset RAIs might be expected in pervasively fractured domes, but longer lasting RAIs would be found in more coherent domes. For both modeled dome geometries, high positive RAIs are formed near the summit while negative RAIs occur at the base of the domes. This indicates that dissolution processes are more

likely during infiltration and precipitation processes are more likely as water percolates out of the base of a dome. In these models, the latter location is occupied by talus, but it could also include features such as brecciated zones at the base of shear lobes/flows (John et al. 2008); for example, the suites of hydrothermal alteration minerals in clay-rich lahars on Mount Rainier are often sourced from brecciated lavas and pyroclastic deposits with high primary permeabilities (Crandell 1971; Scott and Vallance 1995; John et al. 2008). However, because water permeates through domes—which are composed of both fractured lavas and brecciated talus—relatively quickly, it is also possible that the water would not have the opportunity to form advanced alteration assemblages. This is consistent with observations at Santiaguito, where hot springs represent immature waters that have dissolved, but not equilibrated with, dome rock or formed minerals such as clays, and alteration on the dome surfaces is limited to the deposition of hydrous silica (Ball et al. 2013).

These results now provide a framework for investigations of specific mineral formation, for example, by combining temperature and flux data with aqueous geochemical data using a species model such as EQ3/6 (Wetzel et al. 2001). The

Fig. 6 **a**–**h** RAI patterns for crater-confined and perched domes at 1-, 10-, 50-, and 100-year intervals. RAI magnitude scales differ between the two dome geometries, but *warm colors* indicate positive RAIs (dissolution) and *cool colors* indicate negative RAIs (precipitation) in both
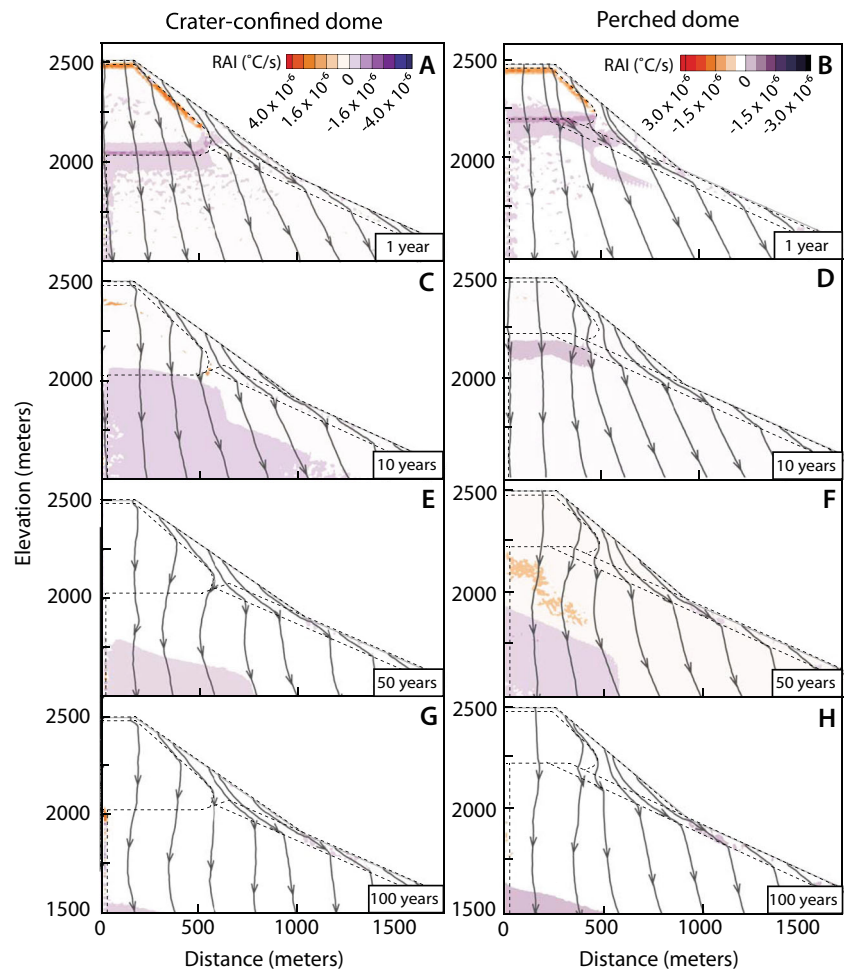
simulation results suggest that alteration minerals forming from dissolution processes (clays and kaolinite) are more likely to be found at the dome summit, while minerals resulting from precipitation processes (alunite) are more likely found at the base of the dome and talus around the slope break. Clays and alunite could contribute to shallow-seated collapses of the carapace and in the talus. Collapses triggered by talus erosion and dome undermining have been associated with intense rainfall (Calder et al. 2005). It might be that increased fluid pressure in clay-bearing horizons contributes to increased instability associated with precipitation. In sufficient quantity, clays, alunite, and silica minerals could also form impermeable layers, facilitating gas sealing (Elsworth et al. 2004), a mechanism that has been suggested for some deep-seated dome failures in active lava domes. Precipitation of vapor-phase cristobalite in domes has been shown to decrease porosity (and by inference, also permeability) of dome rock (Horwell et al. 2013). A similar effect could occur in low-temperature systems, such as modeled here, with other mineral precipitates (Fig. 7); however, more complex models accounting for factors such as fracture networks and high-

permeability zones such as shear lobe boundaries would be necessary for a complete evaluation of this scenario.

The presence of hot, magmatic acidic gases rising from a magma source will accelerate alteration of the dome rock (Reyes 1990). However, Cox and Browne (1998) note that large-scale alteration of rock to smectite/montmorillonite is still possible even in neutral to alkaline pH systems.
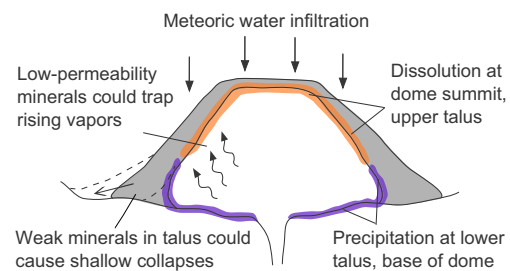

Fig. 7 Summary of dome alteration and potential collapse loci based on RAI patterns. Alteration mineral formation is most likely to occur at the talus/core interface early in the lifetime of the dome and, depending on the mineral species involved, could either strengthen or weaken the dome and/or promote internal gas pressurization

Additionally, while advanced argillic alteration contains a suite of weak sulfate minerals (such as alunite and jarosite) that require the presence of sulfur gases to form, clay minerals such as smectite also depend on the presence of water. Water vapor is the primary gas released in any volcanic eruption and meteoric water composes a significant percentage of the fluid available in any near-surface hydrothermal system (Goff and Janik 2000), and it is reasonable to assume that the degassing pathways followed by water vapor would be, at the shallow levels depicted in these models, essentially the same as those traveled by acidic gases released from a magmatic body. The behavior of water and water vapor is therefore useful both as first-order information and as proxies for interpretations about additional gases in lava dome hydrothermal systems.

Comparison to existing domes and volcanoes

These simulations represent a first-order approach into estimating the behavior of liquid water and water vapor in the interior of cooling lava domes. Physically validating this assessment of alteration is somewhat difficult, since there is currently little in the way of direct or remotely sensed field data about the hydrothermal systems of lava domes. Physical mapping of dissected domes (Duffield et al. 1995; Riggs and Carrasco-Nunez 2004) is generally limited to structural features or eruptive facies and neglects information about alteration mineral assemblages or the location of hydrothermal flow paths or fumaroles. Remote sensing is necessarily limited to surface materials, and while debris avalanches may sample the interior of domes, the percentages and types of altered material involved in volcanic collapses have not been recorded in a systematic or detailed manner in most studies (Dufresne 2009 and personal communication). Voight et al. (2002) were able to trace hydrothermally altered material in the 1996 collapse of the Soufriere Hills lava dome to the margins of the dome and buttressing crater wall, suggesting that permeability contrasts did indeed come into play (the altered material included pyroclastic deposits of brecciated lava). However, in large collapses, the deposits may consist of entire lava domes, making it difficult, if not impossible, to reconstruct internal structures and zones of alteration. As a result, the best available data about undisturbed dome interiors comes from geophysical investigations.

Nicollin et al. (2006) completed an electrical tomographic study of La Soufrière of Guadeloupe volcano and lava dome and created cross sections of electrical resistivity indicating likely areas of hydrothermal alteration (altered materials tend to be less resistive/more conductive). They determined that there was a large area of low resistivity located at the base of the dome, which they interpreted as a hydrothermally altered zone; in addition, a medium resistivity layer on the western flank of the lava dome was found at a depth below a layer of lower resistivity. Other zones of low resistivity were interpreted as cross-cutting faults which provided pathways for liquids and gases that promoted alteration. The authors interpreted the basal layer as related to the collapse of a highly altered summit of the volcano (producing the crater in which the dome formed), but mentioned that the western low-resistivity zone could represent massive unaltered areas of the lava dome overlaid by a layer of thick better drained scoriaceous or altered material from the dome carapace or brecciated units formed during the formation of flow lobes. This would be consistent with the RAI interpretations reached in this model, where alteration is likely to be concentrated at the interface between higher and lower permeability regions (higher permeabilities allow the passage of more liquid and vapor, which are essential to alteration processes). A recently published study by Brothelande et al. (2014) expands on this, indicating that hydrothermal ascending flows in the volcano are limited to the dome and its immediate proximity, confined in a collapse structure surrounding the dome (last modified in 1530 by a collapse followed by an eruption).

Finn et al. (2007) and Finn and Deszcz-Pan (2011) conducted helicopter magnetic and electromagnetic surveys of Mounts Adams and Baker in order to determine the three-dimensional geometry of altered and saturated regions within those Cascade stratovolcanoes. Hydrothermal alteration significantly reduces the magnetization in volcanic rocks, while the presence of alteration minerals, or of water in the rock, reduces electrical resistivity; by combining these methods, the authors were able to discriminate areas of dry, fresh rock from saturated fresh or weakly altered rock and variably intensely altered rock (Finn et al. 2007; Finn and Deszcz-Pan 2011). On Mount Adams, intensely altered and saturated rock is found in the core of the volcano, but layers of fresh or weakly altered saturated rock also underlie portion of the volcano's slopes. The authors interpreted these as "fresh porous breccias," similar to the kind of material found in talus units at lava domes (Finn et al. 2007). Alteration at Mount Baker follows a different pattern, being restricted to thinner layers beneath the summit crater and fumarole field on the volcano's northeast flank (Finn and Deszcz-pan 2011), but similar unaltered or weakly altered saturated layers underlie its slopes. While these methods were applied on an entire stratovolcano and did not discern features on the scale of lava dome structures, ground-based application of magnetic and electromagnetic surveys could provide that information at the scale of a lava dome. Muon radiography (Tanaka et al. 2007; Lesparre et al. 2012) is an emerging geophysical method which shows promise in determining density contrasts in lava domes, but it would be necessary to determine if altered material showed significant density contrasts with unaltered material, and if it was distinguishable from density differences in dome/conduit/talus material in the first place. Currently, muon radiography studies have been able to locate conduits within and beneath domes, but are limited by the fact that the method must

encompass the whole thickness of the dome and cannot take a "slice" from it as in resistivity studies.

In order to corroborate the results of this study, future field and geophysical investigations of both old and young domes would be useful, with attention paid to the location, degree, and character of alteration.

Conclusions

This study applies a multiphase porous flow model to determine the flow of water and heat in low-temperature cooling lava domes over 100-year timescales. A number of conclusions can be drawn from these first-order simulations of lava dome hydrothermal systems.

1. The alteration potential in these domes is controlled by the contrasts in material permeability and the heat sources driving hydrothermal flow and is highest where permeability contrasts are greatest, particularly at the interface between the less permeable dome core and more permeable talus. This suggests that alteration mineral formation is most likely to occur at the boundaries of lava dome structures.
2. Areas of increased alteration likelihood are sustained longer in low-permeability domes, but are more intense in domes with higher permeabilities and persistent heat sources. A dome without a sustained heat input will cool on geologically short time periods and even faster if its overall permeability is high, denying the opportunity to develop alteration. However, at the low temperatures and high infiltration rates in these simulations, there is no evidence for convection of water in the domes and flow is dominated by gravity, precluding the possibility of long-lived hydrothermal circulation.
3. Potential for dissolution (clay mineral formation) is highest near the summit at the core/talus interface of the simulated domes, while the potential for mineral precipitation (alunite, silica formation) is highest at the base of the domes. If alteration forms weak minerals at the core/talus interface, the area could source shallow-seated collapses of the carapace.

In combination with geophysical and field studies, numerical modeling can provide an important first step in elucidating the behavior of posteruptive volcanic systems. Incorporating the results of numerical models with limited ground-based data and remote sensing can strengthen the interpretations drawn from both and provide valuable insight into dome evolution and hazards. Coupling these first-order flow models with mineral species models and representing more complex dome structures and different fluid chemistries could allow simulations such as these to be used to evaluate potential collapse mechanisms at specific domes. The results of the models presented here provide a framework for future investigations, including field, geochemical, and geophysical, into the way posteruptive lava domes are altered by hydrothermal activity.

References

Aizawa K, Ogawa Y, Ishido T (2009) Groundwater flow and hydrothermal systems within volcanic edifices: delineation by electric self-potential and magnetotellurics. J Geophys Res 114:1–12. doi:10.1029/2008JB005910

Alt-Epping P, Smith L (2001) Computing geochemical mass transfer and water/rock ratios in submarine hydrothermal systems: implications for estimating the vigour of convection. Geofluids 1:163–181. doi:10.1046/j.1468-8123.2001.00014.x

Anderson S, Arthur M, Asimow P et al (1999) Encyclopedia of volcanoes. 1442

Ball JL, Calder ES, Hubbard BE, Bernstein ML (2013) An assessment of hydrothermal alteration in the Santiaguito lava dome complex, Guatemala: implications for dome collapse hazards. Bull Volcanol 75:676. doi:10.1007/s00445-012-0676-z

Barclay J, Johnstone JE, Matthews AJ (2006) Meteorological monitoring of an active volcano: implications for eruption prediction. J Volcanol Geotherm Res 150:339–358. doi:10.1016/j.jvolgeores.2005.07.020

Barmin A, Melnik O, Sparks RSJ (2002) Periodic behavior in lava dome eruptions. Earth Planet Sci Lett 199:173–184

Bartetzko A, Klitzsch N, Iturrino G et al (2006) Electrical properties of hydrothermally altered dacite from the PACMANUS hydrothermal field (ODP Leg 193). J Volcanol Geotherm Res 152:109–120. doi:10.1016/j.jvolgeores.2005.10.002

Bedrosian PA, Unsworth MJ, Johnston MJS (2007) Hydrothermal circulation at Mount St. Helens determined by self-potential measurements. J Volcanol Geotherm Res 160:137–146. doi:10.1016/j.jvolgeores.2006.09.003

Bernard ML, Zamora M, Géraud Y, Boudon G (2007) Transport properties of pyroclastic rocks from Montagne Pelée volcano (Martinique, Lesser Antilles). J Geophys Res Solid Earth 112:1–16. doi:10.1029/2006JB004385

Boudon G, Villemant B, Komorowski J et al (1998) The hydrothermal system at Soufriere Hills Volcano, Montserrat (West Indies): characterization and role in the on-going eruption. Geophys Res Lett 25:3693. doi:10.1029/98GL00985

Brace WF (1984) Permeability of crystalline rocks: new in situ measurements. J Geophys Res 89:4327. doi:10.1029/JB089iB06p04327

Brothelande E, Finizola A, Peltier A et al (2014) Fluid circulation pattern inside La Soufrière volcano (Guadeloupe) inferred from combined electrical resistivity tomography, self-potential, soil temperature and diffuse degassing measurements. J Volcanol Geotherm Res 288:105–122. doi:10.1016/j.jvolgeores.2014.10.007

Calder ES, Luckett R, Sparks RSJ, Voight B (2002) Mechanisms of lava dome instability and generation of rockfalls and pyroclastic flows at

Soufriere Hills Volcano, Montserrat. Geol Soc Lond Mem 21:173–190. doi:10.1144/GSL.MEM.2002.021.01.08

Calder ES, Cortés JA, Palma JL, Luckett R (2005) Probabilistic analysis of rockfall frequencies during an andesite lava dome eruption: the Soufrière Hills Volcano, Montserrat. Geophys Res Lett 32:1–4. doi:10.1029/2005GL023594

Carrasco-Núñez G, Díaz-Castellón R, Siebert L et al (2006) Multiple edifice-collapse events in the Eastern Mexican Volcanic Belt: the role of sloping substrate and implications for hazard assessment. J Volcanol Geotherm Res 158:151–176. doi:10.1016/j.jvolgeores.2006.04.025

Chaudhuri A, Rajaram H, Viswanathan H et al (2009) Buoyant convection resulting from dissolution and permeability growth in vertical limestone fractures. Geophys Res Lett 36:587–596. doi:10.1029/2008GL036533

Costa A, Melnik O, Sparks RSJ (2007) Controls of conduit geometry and wallrock elasticity on lava dome eruptions. Earth Planet Sci Lett 260:137–151. doi:10.1016/j.epsl.2007.05.024

Cox ME, Browne P (1998) Hydrothermal alteration mineralogy as an indicator of hydrology at the Ngawha geothermal field, New Zealand. Geothermics 27:259–270. doi:10.1016/S0375-6505(97)10015-3

Crandell DR (1971) Postglacial lahars from Mount Rainier Volcano, Washington. US Geol Surv Prof Pap 677:75

Dash ZV (2003) Validation Test Plan (VTP) Results for the FEHM application version 2.21. 76. http://fehm.lanl.gov/pdfs/fehm_vvr.pdf

Dash ZV, Fitzgerald MF, Pollock F (2003) Validation Test Plan (VTP) for the FEHM application version 2.21. 20. http://fehm.lanl.gov/pdfs/fehm_vvp.pdf

Del Potro R, Hürlimann M (2009) The decrease in the shear strength of volcanic materials with argillic hydrothermal alteration, insights from the summit region of Teide stratovolcano, Tenerife. Eng Geol 104:135–143. doi:10.1016/j.enggeo.2008.09.005

Devoli G, Cepeda J, Kerle N (2009) The 1998 Casita volcano flank failure revisited—new insights into geological setting and failure mechanisms. Eng Geol 105:65–83. doi:10.1016/j.enggeo.2008.12.006

Duffield BWA, Richter DH, Priest SS (1995) Physical volcanology of silicic lava domes as exemplified by the Taylor Creek Rhyolite, Catron and Sierra Counties, New Mexico. US Geol Surv Map I-2399, 1:50,000

Dufresne A (2009) Influence of runout path material on rock and debris avalanche mobility: field evidence and analogue modelling. PhD thesis, University of Freiburg, 268

Elsworth D, Voight B, Thompson G, Young SR (2004) Thermal-hydrologic mechanism for rainfall-triggered collapse of lava domes. Geology 32:969. doi:10.1130/G20730.1

Fields R, Soni BK, Thompson JF, et al. (1996) Geological applications of automatic grid generation tools for finite elements applied to porous flow modeling. Numerical Grid Generation in Computational Fluid Dynamics: Methods 1–9

Fink JH, Griffiths RW (1998) Morphology, eruption rates, and rheology of lava domes: insights from laboratory models. J Geophys Res 103:527. doi:10.1029/97JB02838

Fink JH, Pollard DD (1983) Structural evidence for dikes beneath silicic domes, Medicine Lake Highland Volcano. Calif Geol. doi:10.1130/0091-7613(1983)11<458

Finn CA, Deszcz-Pan M (2011) Helicopter magnetic and electromagnetic surveys at Mounts Adams, Baker and Rainier, Washington: implications for debris flow hazards and volcano hydrology. Soc Explor Geophys Glob Meet Abstr 15:3 pp. doi: 10.1190/1.3659065

Finn CA, Deszcz-Pan M, Anderson ED, John DA (2007) Three-dimensional geophysical mapping of rock alteration and water content at Mount Adams, Washington: implications for lahar hazards. J Geophys Res 112:1–21. doi:10.1029/2006JB004783

Flint LE, Buesch DC, Flint AL (2006) Characterization of unsaturated zone hydrogeologic units using matrix properties and depositional history in a complex volcanic environment. Vadose Zone J 5:480. doi:10.2136/vzj2004.0180

García A, Contreras E, Viggiano JC (1989) Establishment of an empirical correlation for estimating the thermal conductivity of igneous rocks. Int J Thermophys. doi:10.1007/BF00503174

Giggenbach W (1992) SEG distinguished lecture: magma degassing and mineral deposition in hydrothermal systems along convergent plate boundaries. Econ Geol

Goff F, Janik CJ (2000) Geothermal systems. In: Sigurdsson H, Houghton B, McNutt SR et al (eds) Encycl. Volcanoes. Academic Press, San Diego, pp 817–834

Hale AJ (2008) Lava dome growth and evolution with an independently deformable talus. Geophys J Int 174:391–417. doi:10.1111/j.1365-246X.2008.03806.x

Hale AJ, Calder ES, Loughlin SC et al (2009a) Modelling the lava dome extruded at Soufriere Hills Volcano, Montserrat, August 2005-May 2006; part I: dome shape and internal structure. J Volcanol Geotherm Res 187:69–84. doi:10.1016/j.jvolgeores.2009.08.014

Hale AJ, Calder ES, Wadge G et al (2009b) Modelling the lava dome extruded at Soufriere Hills Volcano, Montserrat, August 2005-May 2006; part II: rockfall activity and talus deformation. J Volcanol Geotherm Res 187:53–68. doi:10.1016/j.jvolgeores.2009.08.023

Harford CL, Pringle MS, Sparks RSJ, Young SR (2002) The volcanic evolution of Montserrat using 40Ar/39Ar geochronology. Geol Soc Lond Mem 21:93–113. doi:10.1144/GSL.MEM.2002.021.01.05

Hemmings B, Whitaker F, Gottsmann J, Hughes A (2015) Hydrogeology of Montserrat review and new insights. J Hydrol Reg Stud 3:1–30. doi:10.1016/j.ejrh.2014.08.008

Henley RW, Ellis AJ (1983) Geothermal systems ancient and modern: a geochemical review. Earth Sci Rev. doi:10.1016/0012-8252(83)90075-2

Hicks PD, Matthews AJ, Cooker MJ (2009) Thermal structure of a gas-permeable lava dome and timescale separation in its response to perturbation. J Geophys Res 114, B07201. doi:10.1029/2008JB006198

Horwell CJ, Williamson BJ, Llewellin EW et al (2013) The nature and formation of cristobalite at the Soufrière Hills volcano, Montserrat: implications for the petrology and stability of silicic lava domes. Bull Volcanol 75:1–19. doi:10.1007/s00445-013-0696-3

Hurwitz S, Kipp K, Ingebritsen SE, Reid ME (2003) Groundwater flow, heat transport, and water table position within volcanic edifices: implications for volcanic processes in the Cascade Range. J Geophys Res 108:1–19. doi:10.1029/2003JB002565

Hutnak M, Fisher AT, Zühlsdorf L et al (2006) Hydrothermal recharge and discharge guided by basement outcrops on 0.7–3.6 Ma seafloor east of the Juan de Fuca Ridge: observations and numerical models. Geochem Geophys Geosyst. doi:10.1029/2006GC001242

Ikeda R, Kajiwara T, Omura K, Hickman S (2008) Physical rock properties in and around a conduit zone by welllogging in the Unzen scientific drilling project, Japan. J Volcanol Geotherm Res 175:13–19. doi:10.1016/j.jvolgeores.2008.03.036

Ingebritsen SE, Hayba DO (1994) Fluid flow and heat transport near the critical point of H2. Geophys Res Lett 21:2199–2202. doi:10.1002/9780470114735.hawley04378

Ingebritsen SE, Geiger S, Hurwitz S, Driesner T (2010) Numerical simulation of magmatic hydrothermal systems. Rev Geophys 48:1–33. doi:10.1029/2009RG000287

John DA, Sisson TW, Breit GN et al (2008) Characteristics, extent and origin of hydrothermal alteration at Mount Rainier Volcano, Cascades Arc, USA: implications for debris-flow hazards and mineral deposits. J Volcanol Geotherm Res 175:289–314

Join JL, Folio JL, Robineau B (2005) Aquifers and groundwater within active shield volcanoes. Evolution of conceptual models in the Piton de la Fournaise volcano. J Volcanol Geotherm Res 147:187–201. doi:10.1016/j.jvolgeores.2005.03.013

Keating GN (2005) The role of water in cooling ignimbrites. J Volcanol Geotherm Res 142:145–171. doi:10.1016/j.jvolgeores.2004.10.019

Kerle N (2002) Volume estimation of the 1998 flank collapse at Casita volcano, Nicaragua: a comparison of photogrammetric and conventional techniques. Earth Surf Process Landf 27:759–772. doi:10.1002/esp.351

Khaleel R (1989) Scale dependence of continuum models for fractured basalts. Water Resour Res 25:1847. doi:10.1029/WR025i008p01847

Lavigne F, Thouret J, Voight B et al (2000) Lahars at Merapi volcano, Central Java: an overview. J Volcanol Geotherm Res 100:423–456. doi:10.1016/S0377-0273(00)00150-5

Le Friant A, Boudon G, Komorowski JC et al (2006) Potential flank-collapse of Soufriere volcano, Guadeloupe, Lesser Antilles: numerical simulation and hazards. Nat Hazards 39:381–393. doi:10.1007/s11069-005-6128-8

Lesparre N, Gibert D, Marteau J et al (2012) Density muon radiography of La Soufriere of Guadeloupe volcano: comparison with geological, electrical resistivity and gravity data. Geophys J Int 190:1008–1019. doi:10.1111/j.1365-246X.2012.05546.x

Lopez F (2004) Monimiento de sedimentos en el cauce del Rio Samala: Informe Final. Coord Nac Para La Reducc Desastr 37

McGuire W (2003) Volcano instability and lateral collapse. I:33–45

Miller TA, Vessilinov VV, Stauffer PH, et al (2007) Integration of geologic frameworks in meshing and setup of computational hydrogeologic models, Pajarito Plateau, New Mexico. New Mex. Geol. Soc. Guid. Book, 58th F. Conf. Geol. Jemez Mt. Reg. III

Mueller S, Scheu B, Spieler O, Dingwell DB (2008) Permeability control on magma fragmentation. Geology. doi:10.1130/G24605A.1

Nakada S, Shimizu H, Ohta K (1999) Overview of the 1990–1995 eruption at Unzen Volcano. J Volcanol Geotherm Res 89:1–22. doi:10.1016/S0377-0273(98)00118-8

Nicollin F, Gibert D, Beauducel F et al (2006) Electrical tomography of La Soufrière of Guadeloupe volcano: field experiments, 1D inversion and qualitative interpretation. Earth Planet Sci Lett 244:709–724. doi:10.1016/j.epsl.2006.02.020

Ogawa Y, Daimaru H, Shimizu A (2007) Experimental study of post-eruption overland flow and sediment load from slopes overlain by pyroclastic-flow deposits, Unzen volcano, Japan. Géomorphologie Reli Process Environ 237–246. doi:10.4000/geomorphologie.3962

Opfergelt S, Delmelle P, Boivin P, Delvaux B (2006) The 1998 debris avalanche at Casita volcano, Nicaragua: investigation of the role of hydrothermal smectite in promoting slope instability. Geophys Res Lett 33:4. doi:10.1029/2006gl026661, L15305

Platz T, Cronin SJ, Procter JN et al (2012) Non-explosive, dome-forming eruptions at Mt. Taranaki, New Zealand. Geomorphology 136:15–30. doi:10.1016/j.geomorph.2011.06.016

Rad SD, Allègre CJ, Louvat P (2007) Hidden erosion on volcanic islands. Earth Planet Sci Lett 262:109–124. doi:10.1016/j.epsl.2007.07.019

Raffensperger JP, Vlassopoulos D (1999) The potential for free and mixed convection in sedimentary basins. Hydrogeol J 7:505–520. doi:10.1007/s100400050224

Reid ME, Sisson TW, Brien DL (2002) Volcano collapse promoted by hydrothermal alteration and edifice shape, Mount Rainier, Washington. Geology 29:779–782. doi:10.1130/0091-7613(2001)029<0779:VCPBHA>2.0.CO;2

Reyes AG (1990) Petrology of Philippine geothermal systems and the application of alteration mineralogy to their assessment. J Volcanol Geotherm Res. doi:10.1016/0377-0273(90)90057-M

Riggs N, Carrasco-Nunez G (2004) Evolution of a complex isolated dome system, Cerro Pizarro, central México. Bull Volcanol 66:322–335. doi:10.1007/s00445-003-0313-y

Salaün A, Villemant B, Gérard M et al (2011) Hydrothermal alteration in andesitic volcanoes: trace element redistribution in active and ancient hydrothermal systems of Guadeloupe (Lesser Antilles). J Geochem Explor 111:59–83. doi:10.1016/j.gexplo.2011.06.004

Sammel EA, Ingebritsen SE, Mariner RH (1988) The hydrothermal system at Newberry volcano, Oregon. J Geophys Res 93:10,149–10,162

Scheu B, Spieler O, Dingwell DB (2006) Dynamics of explosive volcanism at Unzen volcano: an experimental contribution. Bull Volcanol 69:175–187. doi:10.1007/s00445-006-0066-5

Scott KM, Vallance JW (1995) Debris flow, debris avalanche, and flood hazards at and downstream from Mount Rainier, Washington. Hydrol Investig Atlas 9 (2 sheets)

Scott KM, Vallance JW, Kerle N et al (2005) Catastrophic precipitation-triggered lahar at Casita volcano, Nicaragua: occurrence, bulking and transformation. Earth Surf Process Landforms 30:59–79. doi:10.1002/esp.1127

Sekioka M (1988) Tentative estimate of bulk permeability of basement rocks from heat discharges in a geothermal field. J Volcanol Geotherm Res. doi:10.1016/0377-0273(88)90006-6

Sheridan MF, Bonnard C, Careeno R, et al (1999) Report on the 30 October 1998 rock fall / avalanche and breakout flow of Casita Volcano, Nicaragua, triggered by Hurricane Mitch. Landslide News 1202–1204

Siebert L (2002) Landslides resulting from structural failure of volcanoes. Catastrophic landslides Eff Occur Mech 15:209–235. doi:10.1130/REG15-p209

Smith JV, Miyake Y, Oikawa T (2001) Interpretation of porosity in dacite lava domes as ductile-brittle failure textures. J Volcanol Geotherm Res 112:25–35. doi:10.1016/S0377-0273(01)00232-3

Smithsonian Institution (1991) Unzen Bull Glob Volcanism Netw 16

Sparks RSJ, Barclay J, Calder ES et al (2002) Generation of a debris avalanche and violent pyroclastic density current on 26 December (Boxing day) 1997 at Soufriere Hills Volcano, Montserrat. Geol Soc Lond Mem 21:409–434. doi:10.1144/GSL.MEM.2002.021.01.18

Tanaka HKM, Nakano T, Takahashi S et al (2007) Imaging the conduit size of the dome with cosmic-ray muons: the structure beneath Showa-Shinzan Lava Dome, Japan. Geophys Res Lett 34, L22311. doi:10.1029/2007GL031389

Velázquez E, Gómez-Sal A (2007) Environmental control of early succession on a large landslide in a tropical dry ecosystem (Casita volcano, Nicaragua). Biotropica 39:601–609. doi:10.1111/j.1744-7429.2007.00306.x

Voight B, Elsworth D (1997) Failure of volcano slopes. Geotechnique. doi:10.1680/geot.1997.47.1.1

Voight B, Elsworth D (2000) Instability and collapse of hazardous gas-pressurized lava domes. Geophys Res Lett 27:1–4

Voight B, Komorowski J, Norton GE et al (2002) The 26 December (Boxing day) 1997 sector collapse and debris avalanche at Soufriere Hills Volcano, Montserrat. Geol Soc Lond Mem 21:363–407. doi:10.1144/GSL.MEM.2002.021.01.17

Wadge G, Ryan G, Calder ES (2009) Clastic and core lava components of a silicic lava dome. Geology 37:551–554. doi:10.1130/G25747A.1

Walker JA, Templeton S, Cameron BI (2006) The chemistry of spring waters and fumarolic gases encircling Santa Maria Volcano, Guatemala. Geol Soc Am Spec Pap 412:59. doi:10.1130/2006.2412(04)

Walter TR, Ratdomopurbo A, Aisyah N et al (2013) Dome growth and coulée spreading controlled by surface morphology, as determined by pixel offsets in photographs of the 2006 Merapi eruption. J Volcanol Geotherm Res 261:121–129. doi:10.1016/j.jvolgeores.2013.02.004

Watanabe T, Shimizu Y, Noguchi N, Nakada S (2008) Permeability measurements on rock samples from Unzen scientific drilling project drill hole 4 (USDP-4). J Volcanol Geotherm Res 175:82–90. doi:10.1016/j.jvolgeores.2008.03.021

Watts RB, Herd RA, Sparks RSJ, Young SR (2002) Growth patterns and emplacement of the andesitic lava dome at Soufriere Hills Volcano, Montserrat. Geol Soc Lond Mem 21:115–152. doi:10.1144/GSL.MEM.2002.021.01.06

Wetzel LR, Raffensperger JP, Shock EL (2001) Predictions of hydrothermal alteration within near-ridge oceanic crust from coordinated geochemical and fluid flow models. J Volcanol Geotherm Res 110:319–342. doi:10.1016/S0377-0273(01)00215-3

Wicks C, de la Llera JC, Lara LE, Lowenstern J (2011) The role of dyking and fault control in the rapid onset of eruption at Chaitén volcano, Chile. Nature 478:374–377. doi:10.1038/nature10541

Zyvoloski G (2007) FEHM: a control volume finite element code for simulating subsurface multi-phase multi-fluid heat and mass transfer. Los Alamos Unclassif. Rep. LA-UR-07-3359

Zyvoloski GA, Robinson BA, Dash ZV, Trease LL (1999) Models and methods summary for the FEHM application. Los Alamos Natl Laboratory Publ SC-194